ACS Catalysis

Research Article

pubs.acs.org/acscatalysis

Carbon Nanotube/Zeolite Hybrid Catalysts for Glucose Conversion in Water/Oil Emulsions

Jimmy Faria,[†] M. Pilar Ruiz,[†] and Daniel E. Resasco*[,‡]

[†]Abengoa Research, Campus Palmas Altas c/Energía Solar n° 1, Palmas Altas, Seville 41014, Spain

[‡]School of Chemical, Biological and Materials Engineering and Center of Interfacial Reaction Engineering (CIRE), University of Oklahoma, Norman, Oklahoma 73019, United States

Supporting Information

ABSTRACT: The isomerization of glucose to fructose and its subsequent dehydration to hydroxymethylfurfural (HMF) have been investigated on nanohybrid catalysts that stabilize emulsions comprising aqueous and organic phases. Significant improvement in catalyst stability was observed when NaX faujasite catalysts were functionalized with multiwalled carbon nanotubes (MWCNT-NaX), with a large fraction of the initial activity and selectivity preserved after several recycles. The combination of MWCNT-NaX, containing Lewis acid sites, and MWCNT-SO_3H, containing Brønsted acid sites, enables glucose isomerization and fructose dehydration at high conversion and HMF selectivity. The use of a water/oil biphasic emulsion favors the continuous separation of the HMF product into the organic phase. Furthermore, selective conversion of HMF into added-value products can be accomplished in the same emulsion by incorporating a metallic function on the amphiphilic nanohybrids in the presence of hydrogen. Depending on the metal used, different final products can be obtained. For example, when Ru was added, the main product was 2,5-hexanedione (47.8 mol %), followed by 2,5-bis(hydroxymethyl)furan (15 mol %) and γ-hydroxyvaleric acid (7.8 mol %). When Pd was used, γ-hydroxyvaleric acid (84 mol %) dominated the product distribution, with only small amounts of 2,5-bis(hydroxymethyl)furan (2.9 mol %).

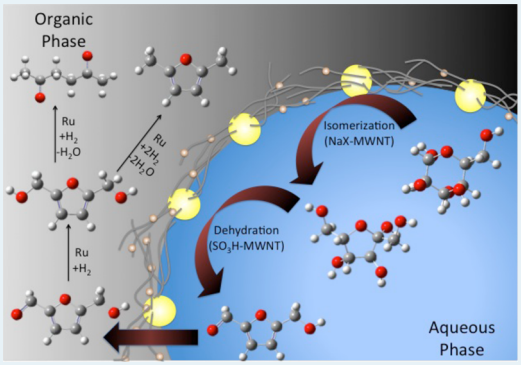

KEYWORDS: *carbon nanotubes, zeolites, glucose, water/oil emulsions*

1. INTRODUCTION

Conversion of biomass-derived carbohydrates to chemical intermediates or fuel components demands a complex multistep process that includes skeletal isomerization, selective removal of excess oxygen atoms, and/or C−C bond formation reactions.[1] Moreover, the typical vapor-phase upgrading used in conventional petrochemical processes is more difficult with carbohydrates due to their low vapor pressure and poor thermal stability.[2] Therefore, liquid-phase processing appears as a necessary approach for these feedstocks. Due to the low solubility of carbohydrates in organic media, polar solvents such as water are required.[3] In most cases, in comparison to organic liquids, water is a desirable solvent due to its relatively reduced cost and reduced environmental impact. However, water generates a severely deactivating environment for many catalytic materials. Dissolution, hydrolysis, and phase transformation phenomena are favored in hot liquid water. High-surface-area catalysts, such as zeolites, are readily converted into amorphous inactive materials in just a few hours. Furthermore, oligomerization and cross-condensation reactions of reactants and products are favored in the aqueous phase and can greatly hinder catalyst activity and selectivity to the desired products. This problem is especially serious in the catalytic upgrading of saccharides in an aqueous environment, since water facilitates the proton transfer reactions, thus increasing the formation of oligomerization products (humins).

Recently, a few examples have been reported demonstrating the enhanced stability of hydrophobized microporous solids in hot liquid water in comparison to their hydrophilic counterparts. Hydrophobization has been accomplished by either minimizing the density of defects in the microporous structure during synthesis or silylating the hydrophilic sites in a postsynthesis treatment.[4−6] For example, Moliner et al.[7,8] have recently explored the use of Sn-β-zeolites with high Si/Al synthesized in HF to reduce the number of terminal defects (Si−OH) and therefore the hydrophilicity of the catalyst, which improves its stability in water. However, due to their high Si/Al ratio, these catalysts can only be used for Lewis acid catalyzed reactions. Alternatively, we have shown that hydrophobization of HY zeolites by functionalization with octadecyltrichlorosilane can greatly increase the catalyst stability in hot liquid water, without sacrificing the Brønsted acid density. In fact, we observed that, even after several cresol alkylation reactions at 200 °C, no significant changes in Brønsted or Lewis acid density occurred.[9,10]

Received: March 21, 2015
Revised: June 27, 2015
Published: July 2, 2015

DOI: 10.1021/acscatal.5b00559
ACS Catal. 2015, 5, 4761−4771

Scheme 1. Integrated Isomerization/Dehydration and Hydrogenation of Cellulosic Biomass: (Left) Glucose Isomerization on Weak Lewis Acid in the Aqueous Phase; (Right) Fructose Dehydration on Brønsted Acid; (Top Right) HMF Hydrolysis on Brønsted Acid Followed by Hydrogenation on Pd To Produce γ-hydroxyvaleric Acid; (Bottom Right) Hydrogenolysis/ Hydration of HMF on Ru To Produce 2,5-Hexanedione

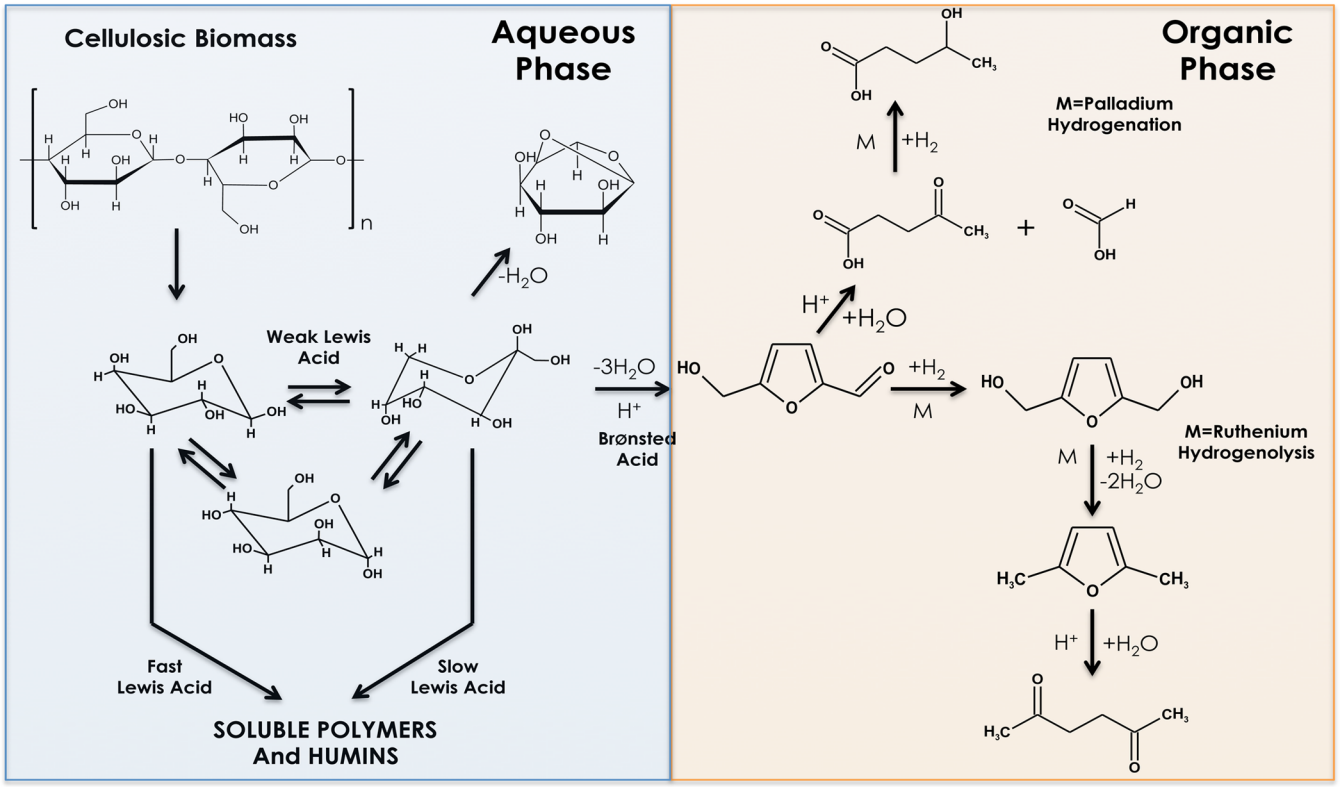

In this contribution, we present a novel technique that benefits from the hydrophobic character of multiwalled carbon nanotubes (MWCNT), which when grown over zeolites improve their tolerance to hot liquid water during carbohydrate upgrading. In recent work, we have demonstrated that this type of nanohybrid particle, comprising carbon nanotubes (SWCNT or MWCNT) fused to metal oxides (SiO_2, Al_2O_3, and MgO) can simultaneously stabilize emulsions and catalyze biofuel upgrading reactions at the water/oil interface.[11−15] Moreover, we have shown that, by adjusting the surface functionality of the nanoparticles, we can systematically control the type of emulsion obtained (i.e., water in oil or oil in water) and particle size distribution of the catalytic metal clusters with high reproducibility. The concept of using these catalytic nanohybrids has the potential to give significant benefits over conventional catalysts for reactions conducted in biphasic liquid systems. In the first place, reaction and separation can be simultaneously accomplished by taking advantage of differences in solubility of reactants and products. By continuously extracting products from the aqueous phase into the organic phase immediately after formation, one can suppress undesired side reactions.[16,17] In addition, emulsification greatly enhances the liquid/solid/liquid interfacial area. Finally, working with catalytic nanohybrids, one can selectively convert molecules in only one of the liquid phases (i.e., phase selectivity), simply on the basis of the differences in solubility and controlling the relative rates of mass transfer in the two phases.[18,19]

To test these novel hydrophobic catalysts, we have studied the isomerization, dehydration, and hydrogenation of glucose and hydroxymethylfurfural (HMF) in a sequential process of reaction/separation steps in water/oil emulsions stabilized by nanoparticles. NaX faujasite zeolites were hydrophobized by growing carbon nanotubes on their surface. As illustrated in Scheme 1 (left), the zeolite catalyzes the isomerization reaction of glucose to fructose. At the same time, the sulfonated multiwalled carbon nanotubes (MWCNT-SO_3H) attached to the zeolite act as Brønsted acid catalysts for the dehydration of fructose to HMF. Subsequently, multiwalled carbon nanotubes (MWCNT) surface decorated with Pd or Ru metal clusters can be used for the hydrodeoxygenation of the resulting HMF (Scheme 1, right). Remarkably, it has been found that the functionalization of the NaX faujasite zeolites greatly improves the catalyst stability in hot liquid water. These results, taken together, indicate that this technology could lead to significant techno-economic benefits by eliminating the need for frequent catalyst replacement and expensive purification methods.

2. EXPERIMENTAL METHODS

2.1. Catalyst Preparation. A series of different nanostructured materials was investigated and tested as catalysts in the conversion of glucose. Nanohybrids composed of carbon nanotubes grown on faujasite NaX zeolites (MWCNT-NaX) were used as catalysts for glucose isomerization, whereas sulfonated multiwalled carbon nanotubes (MWCNT-SO_3H) were employed as catalysts for dehydration. In addition, nanohybrids composed of multiwalled carbon nanotubes fused onto alumina particles (MWCNT-Al_2O_3) functionalized with Pd and Ru catalyst metal clusters were studied as catalysts for the hydrogenation of hydroxymethylfurfuraldehyde (HMF), derived from the isomerization/dehydration of glucose.

DOI: 10.1021/acscatal.5b00559
ACS Catal. 2015, 5, 4761−4771

2.1.1. MWCNT- and SWCNT-NaX Nanohybrid Catalysts for Isomerization of Glucose. Zeolite NaX with a Si/Al ratio of 1.3 and an average particle size of 2 μm was obtained from Sigma-Aldrich. Chemical vapor deposition of carbon-containing molecules (CO or ethylene)[20,21] was respectively used to incorporate hydrophobic SWCNT or MWCNT onto the zeolite. Since the synthesis of nanotubes requires the presence of a metal catalyst (e.g., Co, Mo, Fe),[20,21] the zeolite support was impregnated by the incipient wetness impregnation (IWI) method with aqueous solutions of the appropriate metal salts. That is, for the MWCNT, the salts were $Co(NO_3)_2{\cdot}6H_2O$ and $Fe(NO_3)_3{\cdot}9H_2O$ (Sigma-Aldrich), reaching a final metal loading of 2 wt %, with a Fe/Co molar ratio of 2/1. For the SWCNT, the salts were $Co(NO_3)_2{\cdot}H_2O$ and $(NH_4)_6Mo_7O_{24}{\cdot}4H_2O$ (Sigma-Aldrich), with a final metal loading of 5 wt % and a Co/Mo molar ratio of 1/3. The impregnated samples were dried overnight at 373 K and calcined in air for 2 h at 723 K. After the samples were cooled, 300 mg of the catalyst was placed in a reactor, where it was first reduced under 300 sccm of H_2 at 773 K for 30 min and then heated to 973 K under 300 sccm of He and finally exposed to a flow of gaseous reactant. To obtain the SWCNT, the CoMo/NaX catalyst was exposed to a CO/He flow (4000/2400 sccm), while to obtain MWCNT the FeCo/NaX catalyst was exposed to an ethylene/He flow (500/300 sccm).

2.1.2. MWCNT-SO_3H Catalyst for Dehydration Reaction. Purified multiwalled carbon nanotubes (MWCNT-p) were provided by SouthWest NanoTechnologies Inc. The sulfonic functionalization of the MWCNT-p was performed following a procedure described in the patent literature.[22] Initially, 1 g of MWCNT-p was treated with 50 mL of nitric acid (HNO_3, 16 M) with stirring for 3 h at 393 K. The resulting product was cooled to room temperature and then filtered using nylon filters of 0.22 μm pore size. The collected solids were repeatedly washed with deionized water until neutral pH was reached. The oxidized (acid-treated) multiwalled carbon nanotubes (MWCNT-COOH) were dried overnight at 343 K in a vacuum oven. Then, 1 g of MWCNT-COOH was added to a mixture of 20 mL of sulfuric acid (H_2SO_4, 18 M) and 300 mL of acetic anhydride ($(CH_3CO)_2O$), with continuous stirring, at 353 K. After 2 h, the reaction mixture was cooled to room temperature; the resulting slurry was filtered and thoroughly washed with deionized water to remove any residual acid and finally heated overnight in a vacuum oven at 343 K.

2.1.3. Hydrogenation Catalysts (Pd-MWCNT-Al_2O_3 and Ru-MWCNT-Al_2O_3). Multiwalled carbon nanotubes fused to aluminum oxide (MWCNT-Al_2O_3) were provided by South-West NanoTechnologies Inc. (Norman, OK). These nanohybrids were used as supports of Pd (or Ru) metal particles to catalyze hydrogenation reactions. Metals were incorporated by incipient wetness impregnation of their corresponding precursors ($Pd(NO_3)2{\cdot}6H_2O$ and $RuCl_3{\cdot}6H_2O$, respectively). The final nominal metal loading was 5 wt % of Pd (or Ru). After impregnation, the catalysts were dried overnight at 373 K and calcined at 673 K for 2 h in He.

2.2. Characterization Techniques. Several techniques were employed to characterize the properties and structure of the nanohybrid catalysts, including thermogravimetric/differential thermal analysis coupled with mass spectroscopy (TG-DTA-MS), diffuse reflectance infrared Fourier transformation spectroscopy (DRIFT), X-ray photoelectron spectroscopy (XPS), X-ray diffraction (XRD), N_2 physisorption, and high-resolution transmission electron microscopy (HRTEM), as described below.

2.2.1. Thermogravimetric/Differential Thermal Analysis Coupled with Mass Spectroscopy (TG-DTA-MS). Thermogravimetric analysis of the sulfonic functionalized MWCNT was conducted with Netzsch STA 449 F3 Jupiter TG-DSC equipment, under a flow of air (50 mL/min). First, the sample was kept at 373 K for 30 min and then heated to 1073 K at 10 K/min and finally cooled to 673 K at a rate of 20 K/min. The TGA unit was coupled with an Aëolos mass spectrometer in SIM mode to analyze the outlet gas phase composition during the experiment.

2.2.2. Diffuse Reflectance Infrared Fourier Transformation Spectroscopy (DRIFT). Diffuse reflectance infrared Fourier transformation (DRIFT) spectra were recorded in a high-temperature DRIFT cell (HVC, Harrick) with CaF_2 windows. The sample powder (100 mg) was loaded on the sample cup of the cell; the background spectrum was recorded under room conditions, and then the DRIFT spectra were recorded at a resolution of 4 cm^{-1}, accumulating 256 scans in each measurement.

2.2.3. X-ray Photoelectron Spectroscopy (XPS). X-ray photoelectron spectra were recorded on a Physical Electronics PHI 5800 ESCA system equipped with standard non-monochromatic Al X-rays (1486.6 eV) operated at 250 W and 15 kV in a chamber pumped down to a pressure of approximately 1.0×10^{-8} Torr. Pass energies of 93.9 and 58.7 eV were typically used for survey and specific element analysis, respectively. The electron takeoff angle was 45° with respect to the sample surface. The binding energies were corrected with reference to the C(1s) peak at 284.8 eV. Samples were attached to the aluminum stage with a carbon tape. Atomic composition analyses of carbon, oxygen, and sulfur were carried out on each sample.

2.2.4. X-ray Diffraction (XRD). X-ray powder diffraction patterns (XRD) for the untreated NaX faujasite zeolite and the MWCNT-NaX nanohybrid catalysts were collected on a D8 Series II X-ray diffractometer (Bruker AXS), using Cu Kα radiation generated at 40 kV and 35 mA. The scans covered the 2θ range from 10 to 35°.

2.2.5. High-Resolution Transmission Electron Microscopy (HRTEM). HRTEM images were obtained on a JEOL 2010-F field emission intermediate voltage (200000 V) scanning transmission research electron microscope, with a magnification of up to 8000000×. The samples for HRTEM were prepared by dispersing NaX faujasite zeolites and MWNT-NaX nanohybrids in anhydrous ethanol using a Horn sonicator (Fisher Scientific 600W, 20 kHz) at 25% of amplitude for 5 min to produce a suspension. Then, drops of the suspension were loaded on 300 mesh copper grids with holey carbon film.

2.3. Preparation of Nanohybrid-Stabilized Emulsions. Water/oil emulsions stabilized by various nanohybrids were prepared by dispersing 30 mg of nanohybrids in 30 mL of a 1/1 (v/v) biphasic mixture of the aqueous and organic solvents. The mixture was then sonicated with a Horn sonicator, operating at 25% of amplitude, for 30 min. The emulsions were used for the dehydration of glucose/fructose and the hydrogenation of hydromethylfurfural (HMF); the aqueous and organic phases employed were deionized water and decalin (decahydronaphthalene from Sigma-Aldrich), respectively. In the emulsions used for the isomerization/dehydration reactions, the aqueous and organic phases were 35 wt % NaCl in H_2O and tetrahydrofuran (THF, 99.9 wt % from Sigma-

DOI: 10.1021/acscatal.5b00559
ACS Catal. 2015, 5, 4761−4771

Aldrich), respectively. The high NaCl concentration was used to reduce the solubility of HMF in the aqueous phase and enhance its recovery in the organic phase.

2.4. Reaction Rate Measurements. The rates of isomerization, dehydration, and hydrogenation reactions were measured in a 50 mL Parr 4843 reactor, equipped with an internal J-type thermocouple and a CAL 9500P temperature controller from CAL Controls Ltd. (Figures S1 and S2 in the Supporting Information).

2.4.1. Isomerization–Dehydration of Glucose/Fructose. For the dehydration and isomerization reactions, conducted in batch mode in single liquid phase, a suspension of 200 mg of nanohybrid catalyst in 20 mL of deionized water was placed in the reactor. The system was pressurized to 2.76 MPa in N_2 at room temperature and then heated to 383 K. The reaction started upon injection of 10 mL of glucose aqueous solution from a pressurized container. The resulting initial concentration of glucose inside the reactor was 10 wt %. To stop the reaction, heating and stirring were stopped and the reactor quickly cooled.

For the biphasic experiments, nanohybrid-stabilized emulsions were obtained prior to assembling the reactor, as described above. As in the case of single phase, the biphasic reactions were performed at 2.76 N_2 of pressure and 423 K. At the end of the reaction period, the mixture was filtered using a nylon filter (0.2 μm pore size), which breaks the emulsion and results in a clean separation of the two phases. The samples were then analyzed by high-performance liquid chromatography (HPLC) on a Waters Millipore system (Waters Corp.) equipped with 486 Waters UV (320 nm) and 410 Waters refractive index detectors. Glucose, fructose, and hydroxymethylfurfural concentrations were measured using a Biorad Aminex HPX87C (300 × 7.8) column (Phenomenex), with ultrapure water (pH 7) as the mobile phase at a flow rate of 0.60 mL/min and a column temperature of 353 K. All of the reactants and products were calibrated with commercial standards. Conversion of glucose and selectivities are defined as follows:

$$\text{conversion of glucose} = \frac{\text{moles of glucose reacted}}{\text{moles of glucose initial}} \times 100 \quad (1)$$

$$(\text{yield of product})_i = \frac{(\text{moles of product})_i}{\text{moles of glucose initial}} \times 100 \quad (2)$$

2.4.2. Hydrogenation of Hydroxymethylfurfural. Hydrogenation reaction rates were conducted in a biphasic system containing 5 wt % Pd-MWCNT-Al_2O_3 or 5 wt % Ru-MWCNT-Al_2O_3 catalysts and operating in semibatch mode. In each experiment, 30 mg of catalyst was suspended in 30 mL of a 1/1 deionized water/decalin mixture and sonicated for 15 min using a Horn sonicator in order to produce the emulsion. After the emulsion was placed in the reactor, the system was purged with N_2 and a flow of 110 sccm of pure H_2 at 1.38 MPa was passed during 3 h at 373 K to reduce the metal catalyst. Before the reactant was injected (a solution of 0.03 M hydroxymethylfurfural in water), the temperature was adjusted to 423 K and the H_2 pressure to 2.76 MPa. After 2 h, the reaction was stopped by turning off the heater and switching H_2 to N_2. Once the reaction was finished, the mixture was filtered in two steps, first using a coarse filter paper (8 μm pore size) that collected a large fraction of nanohybrids as they agglomerated upon contacting the filter and, subsequently, using a nylon filter (0.2 μm pore size), which collected the small fraction of nanohybrids that passed the first filter. The two resulting clean phases were separated, and 0.5 mL samples of each were analyzed by GC-FID and GC-MS chromatography: the former was a analyzed on a 6890A series instrument from Agilent Technologies with a capillary column of polyethylene glycol (HP-INNOWAX) of 60.0 m × 0.32 mm × 0.25 μm nominal from Hewlett-Packard and the latter on a Shimadzu QP2010S instrument equipped with an HP-INNOWAX polyethylene glycol capillary column, 30.0 m long × 0.25 μm nominal, from Hewlett-Packard. In all of the GC-FID analyses, methanol and 1,2-dichloroethane were used as internal standards for the aqueous and organic phases, respectively. The reactants and products were calibrated in the GC-FID, using commercial standards. To minimize the damage of the chromatographic column, all aqueous fractions were extracted in methanol before injecting them into the GC.

3. RESULTS AND DISCUSSION

3.1. Particle-Stabilized Emulsions. As demonstrated in previous contributions,[23,15] the ability of different nanohybrids to stabilize water/oil emulsions with large interfacial surface areas is a key parameter in reactions catalyzed at the liquid/liquid interface. Figure 1a illustrates the stability of amphiphilic particles at the liquid/liquid interface of the decalin/water system. Upon sonication, highly stable and reproducible particle-stabilized emulsions can be obtained (Figure 1b). In this process, the emulsion is kinetically stable and is characterized by (1) formation of a layer of particles, at the liquid/liquid interface, that is rigid enough to suppress the coalescence of droplets by steric obstruction[24−27] and (2) modification of the rheological properties (e.g., viscosity) of the liquid that retards the drainage away from coalescent droplets.[28,29] Representative microscopy images of the characteristic emulsions formed when using the sulfonated multiwalled carbon nanotubes (MWCNT-SO_3H) and multi-

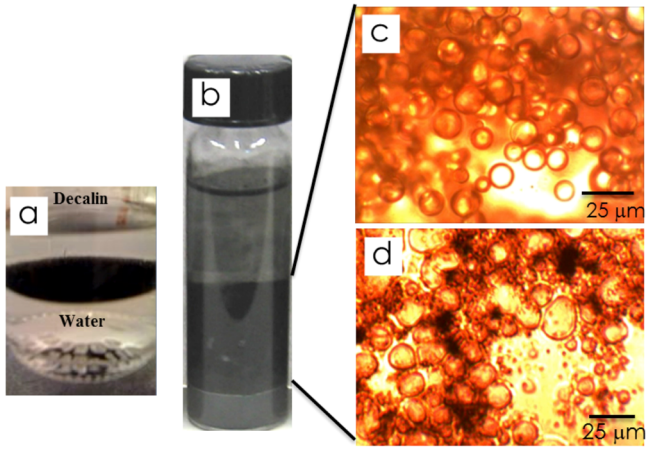

Figure 1. (a) Preferential adsorption of nanohybrids at the water/oil interface in a water/decalin biphasic system with 1 mg/mL of MWNT-SO_3H. (b) The same mixture as in (a) but after horn sonication for 15 min at 25% amplitude. (c) Optical microscope image of the water/decalin (1/1) emulsion stabilized by MWNT-SO_3H (1 mg/mL). (d) Optical microscope image of the water + NaCl (35 wt %)/THF (1/1) emulsion stabilized by MWNT-NaX (6.7 mg/mL).

DOI: 10.1021/acscatal.5b00559
ACS Catal. 2015, 5, 4761−4771

walled carbon nanotubes fused to NaX faujasite zeolites (MWCNT-NaX) are shown in Figures 1c,d.

Table 1 summarizes the type of emulsion, droplet size, and emulsion fraction obtained with the two catalytic nanohybrids investigated. It can be noted that in both systems, MWCNT-SO_3H and MWCNT-NaX, the resulting emulsions had similar average droplet sizes (8.7 ± 1.3 and 11.8 ± 4.4 μm, respectively). The fraction of emulsion in the total mixture was slightly larger (71 vol %) for the sulfonated nanohybrid than for the MWCNT-NaX nanohybrid (50 vol %).

Table 1. Type of Emulsion, Average Droplet Size, and Emulsion Fraction for the Different Nanohybrid-Stabilized Emulsions[a]

nanohybrid	type of emulsion	av droplet size (micron)	emulsion fraction (vol %)
MWCNT-SO_3H	o/w	8.7 ± 1.3	71.2
MWCNT-NaX	w/o	11.8 ± 4.4	50.5

[a]The MWNT-SO_3H measurements correspond to a water/decalin (1/1) emulsion with a particle concentration of 1 mg/mL. For MWNT-NaX the emulsion was prepared from an aqueous solution of NaCl (35 wt %) and THF (1/1) with a particle concentration of 6.7 mg/mL.

As expected, the type of emulsion obtained with MWCNT-SO_3H was oil in water (o/w). In our previous studies,[13−15] we demonstrated that the transition from w/o to o/w emulsions could be achieved by adjusting the extent of nanotube functionalization with polar moieties (that is, −COOH, −COH, and −CHO). Likewise, sulfonation causes a significant increase in the density of surface defects, which favors the formation of o/w emulsions. In contrast, the more hydrophobic MWCNT-NaX stabilized the inversed type of emulsion (w/o). It is known[30−34] that for contact angles at the oil/water/solid interface (as measured across the aqueous phase) slightly lower than 90°, the type of emulsion obtained is o/w, while for contact angles slightly greater than 90°, the emulsion type is the opposite (w/o). Hence, it is not surprising that the more hydrophobic surface of MWCNT-NaX generated w/o emulsions.

3.2. Nanohybrid Characterization. A complete analysis of the structure and composition of MWCNT-SO_3H and MWCNT-NaX nanohybrids was obtained by a combination of different characterization techniques, including DRIFTS, TG-DTA-MS, XRD, XPS, SEM, HRTEM, and N_2 physisorption.

3.2.1. DRIFT Analysis of Nanohybrids. Figure 2 shows the DRIFTS spectra of the three types of nanohybrids: purified multiwalled carbon nanotubes (MWCNT-p), oxidized multiwalled carbon nanotubes (MWCNT-COOH), and sulfonated multiwalled carbon nanotubes (MWCNT-SO_3H). Consistent with previously reported data,[35] no detectable transmission bands were observed in the 2500−4000 cm^{-1} range (Figure 2a) for the pristine MWCNT-p. In contrast, a band centered at about 3450 cm^{-1} was clearly evident for the MWCNT-COOH and MWCNT-SO_3H samples. This band is typically assigned to the stretching mode of −OH groups, arising from defects created during functionalization.[36] Further evidence for the species created by functionalization also appears in the lower wavenumber region shown in Figure 2b. MWCNT-SO_3H displays a stretching mode centered at 1732 cm^{-1}, characteristic of conjugated −CO in the carbon framework. Moreover, the functionalization of MWCNT-p with $-SO_3H$ is confirmed by the bands centered around 1223 and 1050 cm^{-1}, which can be ascribed to $-SO_3H$ and −SH functionalities, respectively.[37]

3.2.2. XPS Analysis of Nanohybrids. X-ray photoelectron spectroscopy was used to further characterize the nature of the functional groups on the carbon nanotube surface. The XPS of the C(1s) region for the three samples is shown in Figure 3a. The major peak for all samples appears at around 284.1 eV (sp^2 C) with a nonsymmetrical edge at higher binding energies that is generally assigned to sp^3 carbon atoms.[38] In addition, the weak band at 290 eV, observed for the MWCNT-p and corresponding to $\pi-\pi^*$ shake up satellites of the sp^2 carbon, is even less prominent for the MWCNT-COOH and MWCNT-SO_3H samples. Likewise, a weak band at around 288.1 eV is visible for MWCNT-COOH and somewhat more prominent for MWCNT-SO_3H, as reported in the literature.[39] This band

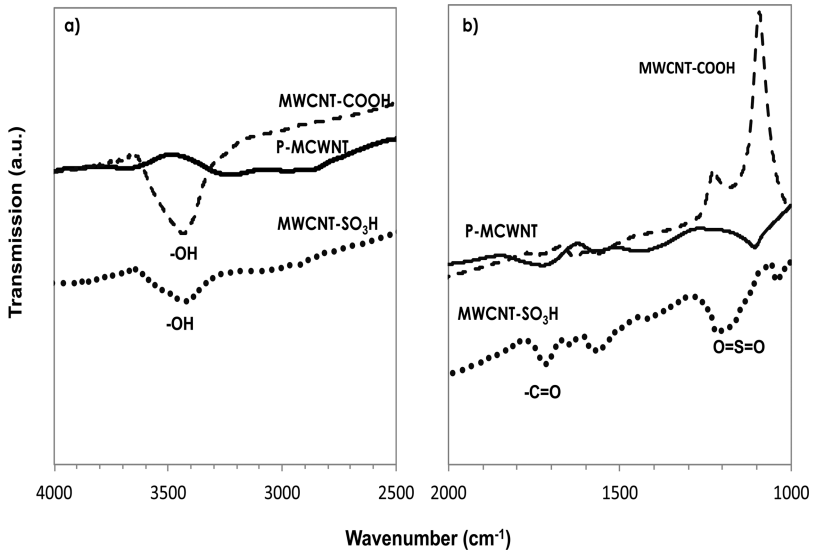

Figure 2. DRIFT spectra of the purified MWNT (p-MWNT), oxidized MWNT (MWNT-COOH), and sulfonated MWNT (MWNT-SO_3H): (a) 4000−2500 cm^{-1} wavenumber region; (b) 2000−1000 cm^{-1} wavenumber region.

DOI: 10.1021/acscatal.5b00559
ACS Catal. 2015, 5, 4761−4771

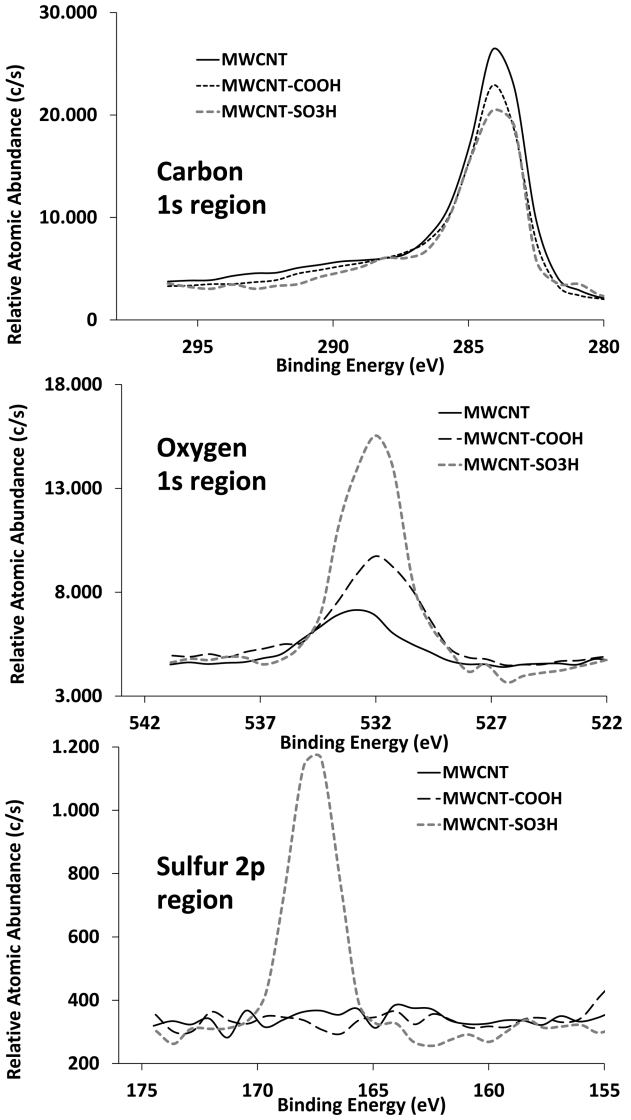

Figure 3. XPS spectra in the regions of (a) C(1s), (b) O(1s), and (c) S(2p) for the MWCNT (p-MWCNT), oxidized MWCNT (MWCNT-COOH), and sulfonated MWCNT (MWNT-SO_3H).

is likely due to carboxylate functional groups ($-COO^-$) formed upon sulfonation.[40,41]

Figure 3b shows the spectra of the O(1s) region. A clear difference between the intensity of the typical band corresponding to O−C at around 532.1 eV was observed between the unfunctionalized and functionalized samples. This band was much more intense for MWCNT-SO_3H and MWCNT-COOH than for the pristine MWCNT-p, particularly for MWCNT-SO_3H, most likely due to the more severe oxidation of the carbon framework upon functionalization with the sulfuric acid and acetic anhydride. On the pristine sample, the band is much weaker and is shifted to around 532.9 eV and is probably associated with H−O−H species, as previously proposed.[42]

As expected, the spectrum of the S(2p) region (Figure 3c) indicates that no sulfur moiety was present in MWCNT-p or MWCNT-COOH, but a clear peak around 167.3 eV was only observed in MWCNT-SO_3H, corresponding to a higher oxidation state of S,[43] indicating the presence of surface oxidized sulfur species covalently bonded to the surface.

The atomic surface composition derived from XPS is summarized in Table S2 in the Supporting Information. It is seen that that the MWCNT-SO_3H sample has about 4% of atomic S on the surface. Likewise, the O content increased from 5.2% in MWCNT-p to 10.3 and 13.8% in MWCNT-COOH and MWCNT-SO_3H, respectively, which is consistent with the extent of surface modification resulting from the different pretreatment methods.

3.2.3. TG-DTS-MS Analysis of Nanohybrids. A TGA system equipped with a mass spectrometer was used to evaluate the thermal stability of the MWCNT-p, MWCNT-COOH, and MWCNT-SO_3H catalysts and simultaneously monitor the evolution of gases as a function of temperature. The thermal analyses were conducted in the 273−1073 K range under an Ar flow (50 mL/min) at a heating rate of 10 K/min. Figure 4a compares the mass loss profiles for the three samples. The MWCNT-p and MWCNT-COOH samples exhibited gradual mass losses from 373 to 1073 K, with totals of around 4 and 12 wt %, respectively. In contrast, the sulfonated MWCNT-SO_3H sample showed a significantly different pattern. The initial weight loss was slow and steady up to about 493 K, similar to the case for the other two samples. However, at this temperature a sharp weight loss was observed, ending up at about 60% of the initial mass. The corresponding evolution of the decomposition products was monitored by MS for the three samples. Figure 4b,c shows that, for the first two samples, desorption of water (below 473 K) and decomposition of oxidized surface groups (i.e., −CO, COOH, −OH, −CHO, and C−O−C) at higher temperatures (>523 K) were responsible for the observed losses. Figure 4d shows that for the MWCNT-SO_3H sample a significant amount of H_2O is evolved at low temperatures but continues to increase with temperature until it reaches a maximum at around 503 K. Likewise, the SO_2, CO_2, and CO MS signals quickly increase at around 491 K, in correspondence with the large mass loss observed in TGA. The initial increase in H_2O and SO_2 signals is due to the decomposition of the $-SO_3H$ functional groups.[44] The CO and CO_2 peaks evolving at 487 K can be associated with the decomposition of the carbonyl moieties on the surface of the carbon nanotubes.[45] The enhanced H_2O evolution of this sample in comparison to the first two could be ascribed to the increased surface hydrophilicity of the CNT upon sulfonation. One important result of relevance to the catalytic activity is that the Brønsted acid sites on the MWCNT-SO_3H hybrid catalysts are thermally stable up to about 493 K, well above the reaction temperatures used in this study.

Table S2 in the Supporting Informationsummarizes the Brønsted acid site density, as determined by the acid−base titration method.[46] Clearly, it was highest for MWCNT-SO_3H (81 mmol/g), while MWCNT-COOH and p-MWCNT had densities of 55.9 and 0.1 mmol/g, respectively.

3.2.4. HRTEM Characterization of Nanohybrids. Further characterization of the structure of the MWCNT-NaX and SWCNT-NaX nanohybrids was obtained by high-resolution transmission electron microscopy (HRTEM). Figure 5 shows microscopy images at two different magnifications for the parent NaX zeolite before the nanotube synthesis (Figure 5a,b) and for the amphiphilic MWCNT-NaX (Figure 5c,d) and SWCNT-NaX (Figure 5e,f). Carbon nanotubes can be seen spanning over the external surface of the faujasite crystallite, which can create a hydrophobic coating. An important observation is the sharp electron diffraction patterns observed in all samples, which indicates that the nanohybrids retain the

DOI: 10.1021/acscatal.5b00559
ACS Catal. 2015, 5, 4761−4771

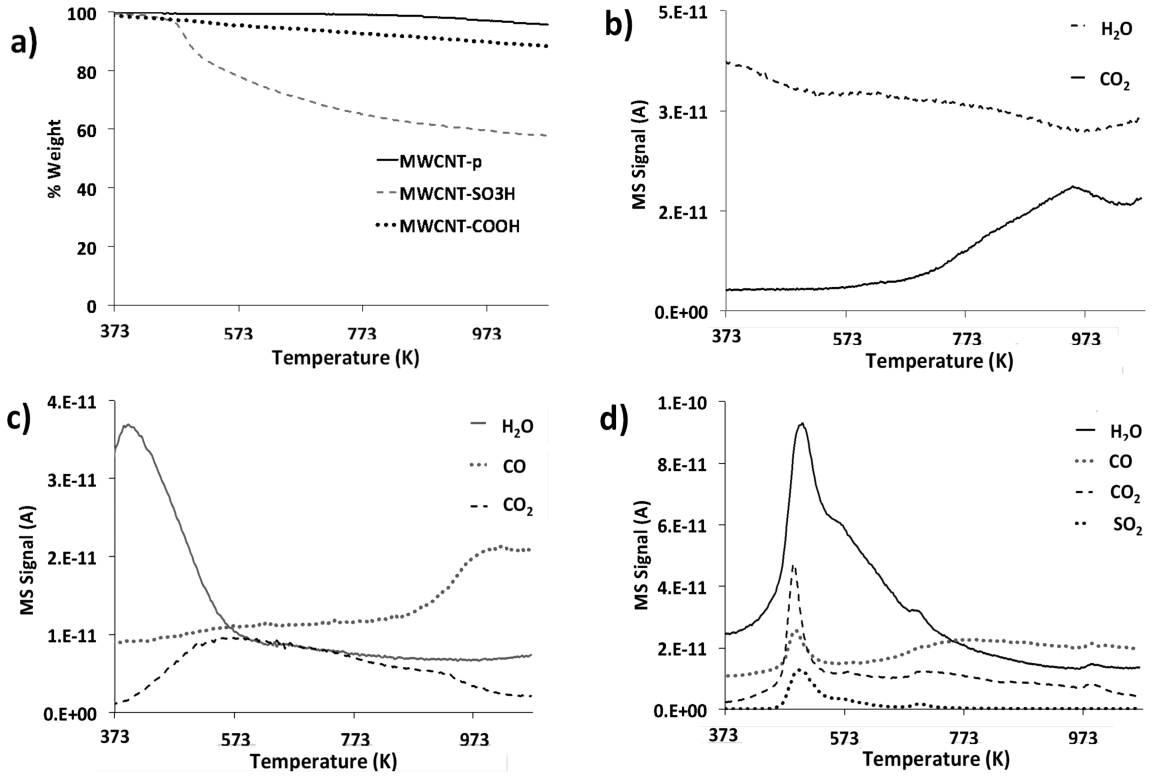

Figure 4. (a) TGA from the nanohybrids purified MWNT (p-MWNT), oxidized MWNT (MWNT-COOH), and sulfonic functionalized MWNT (MWNT-SO_3H). (b–d) MS analysis of (b) purified MWNT (p-MWNT), (c) oxidized MWNT (MWNT-COOH), and (d) sulfonic functionalized MWNT (MWNT-SO_3H).

original crystallinity of the parent zeolite, even after treatment at the high temperature required for the synthesis of the carbon nanotubes.

3.2.5. Raman Spectroscopic Analysis of Nanohybrids. Raman spectroscopy analysis was conducted on the three nanohybrids. This technique has been extensively used to characterize carbon nanotubes.[47−49] Typically, the relative density of defects on carbon nanotubes can be expressed in terms of the intensity ratio of two characteristic bands: the G band, which appears at ∼1590 cm^{-1} and is typically ascribed to the sp^2 carbon atoms of pristine nanotubes, and the D band, which appears around 1350 cm^{-1} and is commonly ascribed to the sp^3 carbon associated with defects.[50−52] Figure 6 shows the normalized Raman spectra and the G/D ratios for -NaX and SWCNT-NaX. As expected, the G/D ratio for SWCNT-NaX (8.73) was significantly higher than that obtained for the MWCNT-NaX (0.95); since SWCNTs are highly pristine, they mainly have sp^2-hybridized carbon atoms, while MWCNTs have a more defective structure with a larger fraction of sp^3-hybridized carbon.

3.3. Glucose Isomerization on MWCNT-NaX and SWCNT-NaX. The glucose isomerization activity of a series of amphiphilic nanohybrid NaX zeolites, that is, functionalized with either SWCNT or MWCNT, was compared to that of the conventional NaX zeolite. As shown in Figure 7, the rate of fructose formation over MWCNT-NaX (26 mol $(kg\ h)^{-1}$) more than twice as high as that on NaX (12 mol $(kg\ h)^{-1}$), while the rate over SWCNT-NaX (12 mol $(kg\ h)^{-1}$) was essentially the same as on the original NaX. The low effectiveness of SWCNT in enhancing activity could be due to the low carbon yield in this sample, which results in low hydrophobicity and, therefore, low stability of the zeolite in the aqueous environment. It is interesting to compare these specific rates previously reported for this reaction. For example, while Sn-β-zeolite exhibits remarkable selectivity and turnover frequency (TOF) per Sn site for glucose isomerization, one limitation of this material is the very low density of Sn sites that can be incorporated before the material becomes unselective. As a result, despite their high TOF, the maximum activity per overall zeolite mass is necessarily low. This limitation of Sn-β-zeolites might become a problem in practical applications. In contrast, while being less active per Na site, the NaX can still be more active per total zeolite mass. The Na^+ ions in the NaX faujasite have a weak Lewis character,[53] which might be responsible for the isomerization activity, as previously proposed.[8] The functionalization with nanotubes makes the zeolite even more effective and stable.

The reusability of MWCNT-NaX catalysts was compared to that of the parent NaX faujasite zeolite in three consecutive 1 h cycles, at 383 K. After each reaction cycle, the catalyst was filtered with a 0.2 μm nylon filter and washed in water and acetone. Then, the catalyst was dried under vacuum at 373 K for 12 h and reused for the isomerization of a freshly prepared 10 wt % glucose solution. As is clearly shown in Figure 8, the rate of glucose conversion greatly decreased after the first cycle on the conventional NaX zeolite; that is, around 85% of the initial activity was lost. In contrast, the MWCNT-functionalized NaX retained almost 70% of its initial activity, even after three reaction cycles. Also, while the fructose product selectivity was greatly affected after the first cycle on the NaX zeolite (i.e. about 38% on the third cycle), it was maintained at around 70% for the three cycles on the nanohybrid MWCNT-NaX catalyst.

To assess the changes in zeolite crystallinity during the reaction cycles, the unmodified NaX and the MWCNT-

DOI: 10.1021/acscatal.5b00559
ACS Catal. 2015, 5, 4761−4771

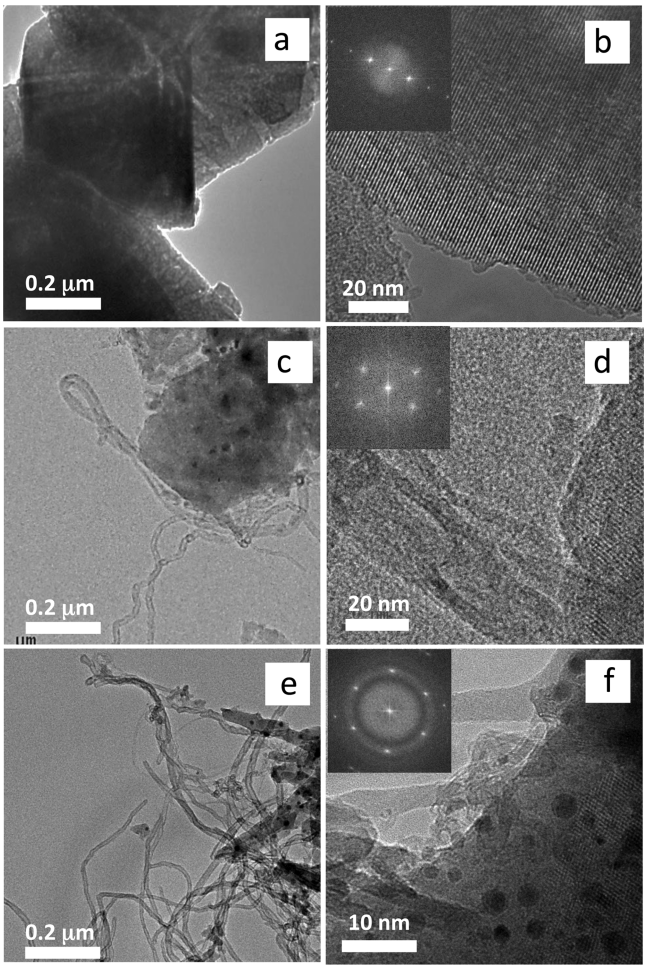

Figure 5. HRTEM images at different magnifications and electron diffraction pattern of the catalytic materials before (a, c, e) and after (b, d, f) synthesis of carbon nanotubes: (a, b) commercial NaX faujasite zeolite; (c, d) MWCNT-NaX; (e, f) SWCNT-NaX.

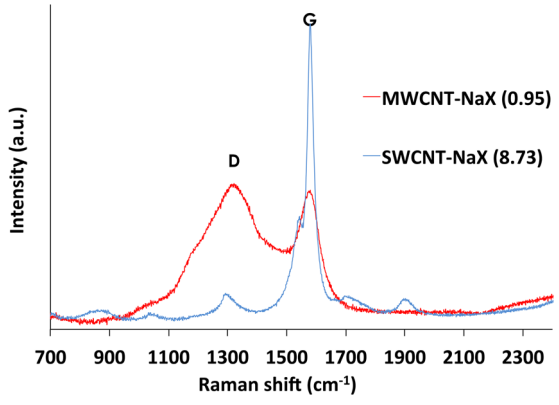

Figure 6. Normalized Raman spectra of the SWCNT-NaX and MWCNT-NaX nanohybrids. The D/G intensity ratios are indicated in parentheses.

functionalized NaX zeolite samples were characterized by XRD before and after 1 h glucose isomerization reactions in the aqueous phase at 383 K and 2.76 MPa of N_2.

As shown in Figure 9, no significant changes were observed in the XRD of the used sample in comparison with the fresh MWCNT-NaX catalyst. However, the diffraction peaks at 25.55 and 27.55°, which correspond respectively to the (551) and

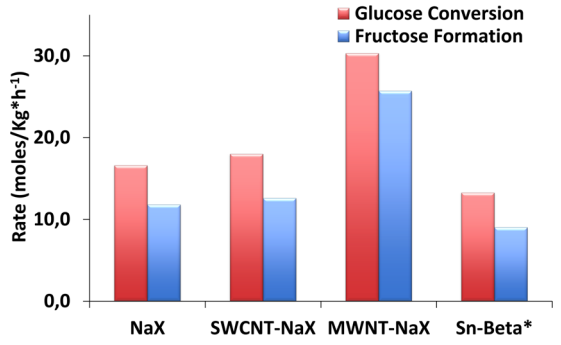

Figure 7. Rates per unit mass of glucose conversion and fructose formation over commercial NaX zeolite, nanohybrid MWNT-NaX, and nanohybrid SWNT-NaX. Conditions: glucose isomerization in the aqueous phase at 383 K, stirring at 600 rpm, 2.76 MPa of N_2, over 200 mg of catalyst; feed 10 wt % glucose, total reaction volume 30 mL. (*) Sn-β-zeolite catalyst at 383 K with a Sn/glucose ratio of 1/50 from ref 10.

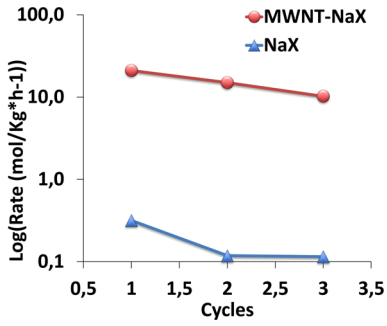

Figure 8. Reusability of the conventional NaX zeolite and the MWNT-functionalized NaX. Conditions: consecutive cycles of glucose isomerization in the aqueous phase at 383 K, 600 rpm of agitation, and 2.76 MPa of N_2 over 200 mg of catalyst; feed 10 wt % of glucose in a total reaction volume of 30 mL. After each reaction cycle, the catalyst was washed with 200 mL of acetone and dried for 12 h in a vacuum oven at 353 K.

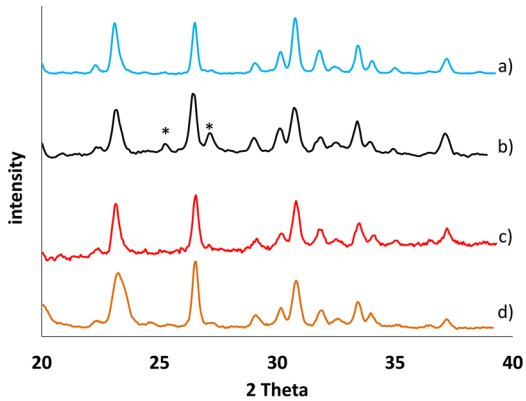

Figure 9. X-ray diffraction of NaX zeolite (a) before and (b) after reaction and MWCN-NaX nanohybrids (c) before and (d) after reaction. The catalysts were treated for 1 h of isomerization reaction of glucose at 383 K, 600 rpm of agitation, and 400 psi of N_2 over 200 mg of catalyst. The concentration of glucose in the reaction was 10 wt %, and the reaction volume was 30 mL.

(331) planes,[54] which are almost imperceptible on the fresh NaX sample, became significant in the used catalyst. Thus, this indicates some degree of modification of the zeolite structure.

DOI: 10.1021/acscatal.5b00559
ACS Catal. 2015, 5, 4761−4771

Further reaction experiments with the MWCNT-NaX catalyst were performed in the aqueous phase at 383 K and

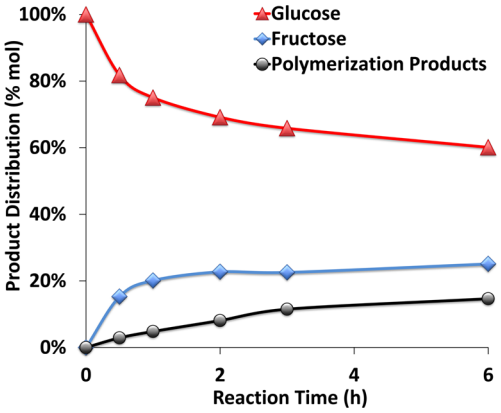

Figure 10. Product distribution form the isomerization reaction of glucose with time in the aqueous phase at 110 °C, 600 rpm of agitation, and 400 psi of N_2 over NaX-MWNT nanohybrid catalyst (200 mg). The feed was 10 wt % of glucose in a total reaction volume of 30 mL.

2.76 MPa of N_2. Figure 10 shows the evolution of the product distribution with reaction time. At low conversions, the fructose selectivity was very high (e.g., around 85% when glucose conversion <20%); however, after 2 h of reaction, the fructose yield reached a plateau while the glucose conversion (disappearance) kept increasing, as polymerization products were formed. The observed additional disappearance of glucose can be ascribed to the heat-catalyzed degradation of saccharides toward soluble polymers and humins, as previously reported by several authors.[55−58]

In the enzymatic process currently used to produce fructose industrially, an equilibrium mixture of 42 wt % fructose, 50 wt % glucose, and 8 wt % of other saccharides is typically obtained.[59,60] However, a higher product efficiency could be obtained if fructose is further converted, for example, to hydroxymethylfurfuraldehyde (HMF), which could be continuously extracted due to its preferential partition into organic solvents. Furthermore, HMF can be further converted in the organic phase to more stable products that can be valuable platforms for the production of fuels or monomers. We have tested this concept using catalytic nanohybrids in emulsions, by dehydrating fructose over Brønsted acid sites anchored on the surface of the functionalized MWCNT. Sulfonic ($-SO_3H$) groups are particularly appealing for this function, since they not only provide strong Brønsted acidity but also exhibit acceptable thermal stability.[61] It has been reported that carbon-based materials bearing sulfonic acid groups have enhanced catalytic activity and stability for the production of biodiesel and cellulose hydrolysis in comparison to conventional solid acid catalysts.

Table 2 shows the evolution of the yield/conversion with time for the dehydration reaction of glucose (10 wt %) at 423 K in a water/decalin emulsion (1/1 volume ratio) stabilized by 1 mg/mL of MWCNT-SO_3H. At this elevated temperature, the yield of the HMF slightly increased with time, while the glucose concentration decreased due to the onset of the polymerization reactions. The formic and levulinic acids formed as results of the hydrolysis of HMF were observed, even at short reaction times. At longer reaction times, the formic acid and levulinic acid reached a maximum yield of 8.2 and 8.6 mol %, respectively.

In sharp contrast, fructose dehydration under the same reactions conditions showed a much more selective conversion toward HMF (Table 2). It can be seen that, at 60 min reaction time (65% conversion), the yield of HMF from fructose was around 32%, almost 10 times higher than the yield observed with glucose at 75% conversion. These differences in HMF selectivity can be ascribed to the relatively low stability of the fructose ring structure in comparison to that of glucose.

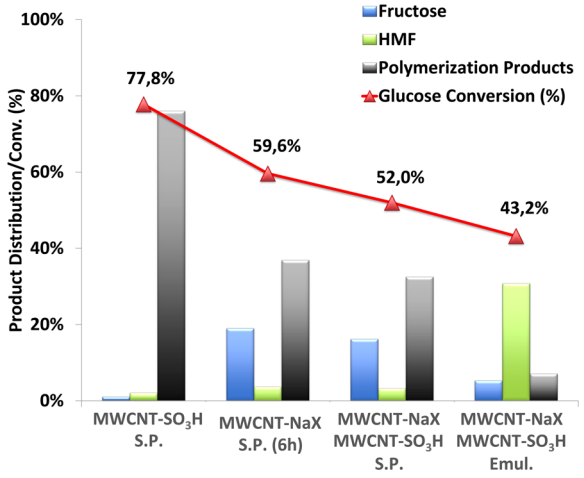

Figure 11. Conversion of glucose and product distribution from the isomerization/dehydration reaction in single phase (S.P.) and in water (35 wt % NaCl)/THF emulsion of glucose (Emul.). Reactions were carried out at 150 °C, 600 rpm of agitation, and 400 psi of N_2 over 200 mg of catalyst. The feed was 10 wt % of glucose in a total reaction volume of 30 mL.

The stability of the six-membered carbon ring of glucose is very high; consequently, the concentration of the open-chain structure in solution is rather low. In contrast, in fructose, the

Table 2. Conversions and Product Distributions Obtained in the Dehydration Reaction of Glucose (or Fructose) at 423 K, 300 rpm of Agitation, and 4.14 MPa of N_2 over 50 mg of Nanohybrid Catalyst (MWNT−SO_3H) in Water/Decalin (1/1 v/v) Emulsion[a]

			product distribution (mol %)		
reactant	reaction time (min)	conversion (%)	5-hydroxymethylfurfural	formic acid	levulinic acid
glucose	30	34.4	1.4	5.0	5.5
	60	76.3	3.5	6.3	6.9
fructose	30	40.1	5.7	4.5	5.2
	60	65.5	31.5	8.2	8.6

[a]Reactant concentration: 10 vol % in 40 mL of total volume.

DOI: 10.1021/acscatal.5b00559
ACS Catal. 2015, 5, 4761−4771

Table 3. Conversion of Hydroxymethylfurfural (HMF) and Product Distribution Obtained in the Hydrogenation Reaction of HMF after 2 h of Reaction at 150 °C, 300 rpm of Agitation, and 600 psi of N_2 over 50 mg of Nanohybrid Catalyst (5% Ru/MWNT/Al_2O_3 and 5% Pd/MWNT/Al_2O_3) in Water/Decalin (1/1) Emulsion[a]

			product distribution (mol %)		
catalyst	HMF conversion (%)	TOF (s^{-1})	2,5-bis(hydroxymethyl) furan	2,5-hexanedione	γ-hydroxyvaleric acid
5% Ru/MWNT/Al_2O_3	70.7	0.25	15.0	47.8	7.8
5% Pd/MWNT/Al_2O_3	87.0	0.34	2.9	0	84.1

[a]Feed: 1 g of hydroxymethylfurfural in 40 mL of total volume.

open-chain structure is dominant. This is especially relevant for the dehydration reaction, since the enolization of the open-chain saccharides is believed to be the rate-limiting step.[62] Additionally, fructose forms difructose dianhydrides that are sterically hindered, making cross-polymerization less favorable than in the case of glucose.[63−66] These molecules contain reducing groups that can react with reaction intermediates and HMF.[67]

To improve the poor selectivity obtained in the dehydration of the sugars in the water/decalin nanohybrid-stabilized emulsions, we coupled isomerization and dehydration reactions by simultaneously incorporating the two catalytic functions at the liquid−liquid interface of the water−oil emulsion. In addition, THF- and NaCl-saturated aqueous solutions (35 wt %) were used to enhance the extractive capacity of the organic solvent. As shown in previous studies,[16,17,68] the partition of HMF in aqueous/organic systems can be greatly shifted toward the organic phase by dissolving NaCl in the aqueous phase. In this case, a remarkable increase in selectivity to HMF (around 71%) was observed when the two nanohybrid catalysts MWCNT-SO_3H + MWCNT-NaX were combined with the NaCl water/THF emulsions. The product distributions obtained in this system after 1 h of reaction at 423 K and 2.76 MPa of N_2 are summarized in Figure 11. For comparison, we also carried out the same reaction in a single aqueous phase. The difference is noteworthy; in this case, the resulting HMF selectivity decreased to a value close to 6%, while the glucose disappearance remained at around 52%. The remarkable enhancement in selectivity to HMF, observed for the nanohybrid-stabilized emulsions, even under relatively harsh conditions, can be ascribed to two main factors: (a) improved aldose-ketose isomerization to fructose, which can selectively dehydrate to HMF, and (b) removal of HMF from the aqueous to the organic phase, thus preventing cross-condensation with the saccharides, even at high levels of conversion.

Finally, we conducted the HMF hydrogenation reaction in water/decalin emulsions to selectively convert the HMF, in the organic phase, to compounds that could be valuable for the production of renewable fuels and polymeric resins. Table 3 summarizes the product distribution obtained after 2 h of reaction of HMF over 5 wt % Ru or Pd supported on MWCNT-Al_2O_3 nanohybrids at 423 K and 4.14 MPa of H_2.

Interestingly, significant differences were observed between the Ru and Pd MWCNT-Al_2O_3 catalysts at comparable levels of conversion (70−90%). In the former, the 2,5-hexanedione was the major product (47.8 mol %), followed by 2,5-bis-(hydroxymethyl)furan (15 mol %) and γ-hydroxyvaleric acid (7.8 mol %). In sharp contrast, the latter showed only two species: the hydrolysis/hydrogenation product (84.1 mol % of γ-hydroxyvaleric acid), and the hydrogenated HMF (2.9 mol % of 2,5-bis(hydroxymethyl)furan). From these results it seems that the rate of C−O hydrogenolysis is much faster on Ru, which increases the yield of 2,5-dimethylfuran (DMF), followed by alkene hydrolysis and ring opening to form 2,5-hexanedione. In the case of the Pd catalyst, the hydrogenation activity is lower, allowing the acid hydrolysis to convert the HMF into levulinic acid and formic acid that then can be hydrogenated to γ-hydroxyvaleric acid and light gases.

4. CONCLUSIONS

In summary, we have demonstrated that a combination of Lewis and Brønsted acid sites, together with a metal function on a hydrophobic support, exhibits improved hydrothermal stability and resistance to leaching of the active sites, which are crucial requirements for large-scale refining of biomass-derived carbohydrates. Conventional NaX faujasite zeolites, in which the sodium ions act as weak Lewis acid sites for the keto-aldose isomerization of glucose, are rapidly deactivated in liquid water at 383 K. In contrast, functionalized MWCNT-NaX zeolite keeps its catalytic activity and crystalline structure in this harsh environment.

Furthermore, the combination of Lewis acid sites (MWCNT-NaX) and Brønsted acid sites (MWCNT-SO_3H) in biphasic aqueous (NaCl 35 wt %)/THF emulsions, greatly enhances the selectivity to desired products. Upon isomerization of glucose to fructose over Lewis acid sites and dehydration over Brønsted acid sites, the resulting HMF rapidly transfers to the organic phase, reaching a selectivity above 70% at conversions close to 60%. In addition, we explored the concept of continuous extraction and selective hydrogenation of HMF in the organic solvent over metal clusters anchored on hydrophobic MWCNT fused to aluminum oxide (metal-MWCNT-Al_2O_3). It was possible to improve the selectivity of the hydrogenation reaction by both preventing the competitive hydrogenation of the sugars in the aqueous phase and producing more stable hydrodeoxygenated molecules such as 2,5-hexadinone and γ-hydroxyvaleric acid, two excellent platform chemicals for several industrial processes.

■ ASSOCIATED CONTENT

Supporting Information

The Supporting Information is available free of charge on the ACS Publications website at DOI: 10.1021/acscatal.5b00559.

Reactor process and instrumentation diagrams (PID), HRTEM characterization of 5 wt % Pd/and Ru/MWCNT/Al_2O_3, and schematic illustration of the reaction system involved in the catalysis in emulsion. (PDF)

■ AUTHOR INFORMATION

Corresponding Author

*D.E.R.: tel, (+1) 405-325-4370; fax, (+1) 405-325-5813; e-mail, resasco@ou.edu.

Notes

The authors declare no competing financial interest.

DOI: 10.1021/acscatal.5b00559
ACS Catal. 2015, 5, 4761−4771

■ ACKNOWLEDGMENTS

Support from the Department of Energy DOE EPSCOR (Grant DE SC0004600) is gratefully acknowledged. The authors thank G. W. Strout of the Samuel Roberts Noble Electron Microscopy for technical support.

■ REFERENCES

(1) Lange, J. P. In *Catalysis for Renewables: From Feedstock to Energy Production*; Centi, G., van Santen, R. A., Eds.; Wiley-VCH: Weinheim, Germany, 2007; Vol. *1*, p 39.
(2) Huber, G. W.; Iborra, S.; Corma, A. *Chem. Rev.* **2006**, *106*, 4044−4098.
(3) Resasco, D. E.; Crossley, S. *AIChE J.* **2009**, *55*, 1082−1089.
(4) Nur, H.; Ikeda, S.; Ohtani, B. *J. Catal.* **2001**, *204*, 402−408.
(5) Meininghaus, C. K. W.; Prins, R. *Microporous Mesoporous Mater.* **2000**, *35-36*, 349−365.
(6) Zhao, X. S.; Lu, G. Q. *J. Phys. Chem. B* **1998**, *102*, 1556−1561.
(7) Bermejo-Deval, R.; Assary, R. S.; Nikolla, E.; Moliner, M.; Román- Leshkov, Y.; Hwang, S. J.; Palsdottir, A.; Silverman, D.; Lobo, R. F.; Curtiss, L. A.; Davis, M. E. *Proc. Natl. Acad. Sci. U. S. A.* **2012**, *109*, 9727−9732.
(8) Moliner, M.; Roman-Leshkov, Y.; Davis, M. E. *Proc. Natl. Acad. Sci. U. S. A.* **2010**, *107*, 6164−6168.
(9) Zapata, P. A.; Faria, J.; Ruiz, M. P.; Jentoft, R. E.; Resasco, D. E. *J. Am. Chem. Soc.* **2012**, *134*, 8570−8578.
(10) Corma, A.; Domine, M. E.; Valencia, S. *J. Catal.* **2003**, *215*, 294−304.
(11) Crossley, S.; Faria, J.; Shen, M.; Resasco, D. E. *Science* **2010**, *327*, 68−72.
(12) Faria, J.; Ruiz, M. P.; Resasco, D. E. *Adv. Synth. Catal.* **2010**, *352*, 2359−2364.
(13) Shen, M.; Resasco, D. E. *Langmuir* **2009**, *25*, 10843−10851.
(14) Prasomsri, T.; Shi, D.; Resasco, D. E. *Chem. Phys. Lett.* **2010**, *497*, 103−107.
(15) Ruiz, M. P.; Faria, J.; Shen, M.; Drexler, S.; Prasomsri, T.; Resasco, D. E. *ChemSusChem* **2011**, *4*, 964−974.
(16) Roman-Leshkov, Y.; Chheda, J. N.; Dumesic, J. A. *Science* **2006**, *312*, 1933−1937.
(17) Roman-Leshkov, Y.; Barrett, C. J.; Liu, Z. Y.; Dumesic, J. A. *Nature* **2007**, *447*, 982−986.
(18) Cole-Hamilton, D. J. *Science* **2010**, *327*, 41−42.
(19) Resasco, D. E. *Chin. J. Catalysis* **2014**, *35*, 798−806.
(20) Alvarez, W. E.; Kitiyanan, B.; Borgna, A.; Resasco, D. E. *Carbon* **2001**, *39*, 547−558.
(21) Resasco, D. E.; Kitiyanan, B.; Harwell, J. H.; Alvarez, W. U.S. Patent No. US6,333,016, 2001.
(22) Bollepalli, S. Sulfonated carbonaceous materials. US Patent US7,241,334, 2007.
(23) Zapata, P. A.; Faria, J.; Ruiz, M. P.; Resasco, D. E. *Top. Catal.* **2012**, *55*, 38−52.
(24) Briggs, T. R. *J. Ind. Eng. Chem.* **1921**, *13*, 1008−1010.
(25) Levine, S.; Sanford, E. *Can. J. Chem. Eng.* **1985**, *63*, 258−268.
(26) Menon, V. B.; Wasan, D. T. *Colloids Surf.* **1987**, *23*, 353−362.
(27) Menon, V. B.; Wasan, D. T. *Sep. Sci. Technol.* **1988**, *23*, 2131−2142.
(28) Tambe, D. E.; Sharma, M. M. *Adv. Colloid Interface Sci.* **1994**, *52*, 1−63.
(29) Johansen, E. J.; Skjarvo, M. I.; Lund, T.; Sjoblom, J.; Soderlund, H.; Bostrom, G. *Colloids Surf.* **1988**, *34*, 353−370.
(30) Finkle, P.; Draper, H. D.; Hilderbrand, J. H. *J. Am. Chem. Soc.* **1923**, *45*, 2780−2788.
(31) Schulman, J. H.; Leja, J. *Trans. Faraday Soc.* **1954**, *50*, 598−605.
(32) Binks, B. P. *Curr. Opin. Colloid Interface Sci.* **2002**, *7*, 21−41.
(33) Binks, B. P.; Lumsdon, S. O. *Langmuir* **2001**, *17*, 4540−4547.
(34) Binks, B. P.; Philip, J.; Rodrigues, J. A. *Langmuir* **2005**, *21*, 3296−3302.
(35) Koshio, A.; Yudasaka, M.; Zhang, M.; Iijima, S. *Nano Lett.* **2001**, *1*, 361−363.
(36) Pompeo, F.; Resasco, D. E. *Nano Lett.* **2002**, *2*, 369−373.
(37) Adams, L.; Oki, A.; Grady, T.; McWhinney, H.; Luo, Z. *Phys. E* **2009**, *41*, 723−728.
(38) Okpalugo, T. I. T.; Papakonstantinou, P.; Murphy, H.; McLaughlin, J.; Brown, N. M. D. *Carbon* **2005**, *43*, 153−161.
(39) Holzinger, M.; Hirsch, A.; Hennrick, F.; Kappes, M. M.; Dziakowa, A.; Ley, L.; Graupner, R. *Am. Inst. Phys. Conf. Proc.* **2002**, *633*, 96−99.
(40) Baker, S. E.; Cai, W.; Kasseter, T. L.; Weidkamp, K. P.; Hamers, R. J. *Nano Lett.* **2002**, *2*, 1413−1417.
(41) Hiura, H.; Ebbesen, T. W.; Tanigaki, K. *Adv. Mater.* **1995**, *7*, 275−276.
(42) Martinez, M. T.; Callejas, M. A.; Benito, A. M.; Cochet, M.; Seeger, T.; Ansón, A.; Schreiber, J.; Gordon, C.; Marhic, C.; Chauvet, O.; Fierro, J. L. G.; Maser, W. K. *Carbon* **2003**, *41*, 2247−2256.
(43) Cano-Serrano, E.; Blanco-Brieva, G.; Campos-Martin, J. M.; Fierro, J. L. G. *Langmuir* **2003**, *19*, 7621−7627.
(44) Hara, M.; Yoshida, T.; Takagaki, A.; Takata, T.; Kondo, J. N.; Hayashi, S.; Domen, K. *Angew. Chem., Int. Ed.* **2004**, *43*, 2955−2958.
(45) Peng, F.; Zhang, L.; Wang, H.; Lv, P.; Yu, H. *Carbon* **2005**, *43*, 2405−2408.
(46) Hu, H.; Bhowmik, P.; Zhao, B.; Hamon, M. A.; Itkis, M. E.; Haddon, R. C. *Chem. Phys. Lett.* **2001**, *345*, 25−28.
(47) Dillon, A. C.; Yudasaka, M.; Dresselhaus, M. S. *J. Nanosci. Nanotechnol.* **2004**, *4*, 691−703.
(48) Musumeci, A. W.; Waclawik, E. R.; Frost, R. L. *Spectrochim. Acta, Part A* **2008**, *71*, 140−142.
(49) Kobayashi, Y.; Takagi, D.; Ueno, Y.; Homma, Y. *Phys. E* **2004**, *24*, 26−31.
(50) Bachilo, S. M.; Balzano, L.; Herrera, J. E.; Pompeo, F.; Resasco, D. E.; Weisman, R. B. *J. Am. Chem. Soc.* **2003**, *125*, 11186−11187.
(51) Simpson, J. R.; Fagan, J. A.; Becker, M. L.; Hobbie, E. K.; Hight, W. A. R. *Carbon* **2009**, *47*, 3238−3241.
(52) Delhaes, P.; Couzi, M.; Trinquecoste, M.; Dentzer, J.; Hamidou, H.; Vix-Guterl, C. *Carbon* **2006**, *44*, 3005−3013.
(53) Shabtai, J.; Lazar, R.; Biron, E. *J. Mol. Catal.* **1984**, *27*, 35−43.
(54) Treacy, M. M. J.; Higgins, J. B. *Collection of Simulated XRD Powder Patterns for Zeolites*, 4th ed.; Elsevier: Amsterdam, 2001.
(55) Qian, X.; Nimlos, M. R.; Davis, M.; Johnson, D. K.; Himmel, M. E. *Carbohydr. Res.* **2005**, *340*, 2319−2327.
(56) Garrett, E. R.; Dvorchik, B. H. J. *J. Pharm. Sci.* **1969**, *58*, 813−820.
(57) Abatzoglov, N.; Bouchard, J.; Chornet, E.; Overend, R. P. *Can. J. Chem. Eng.* **1986**, *64*, 781−786.
(58) Weingarten, R.; Tompsett, G. A.; Conner, C., Jr.; Huber, G. W. *J. Catal.* **2011**, *279*, 174−182.
(59) Tewari, Y. *Appl. Biochem. Biotechnol.* **1990**, *23*, 187−203.
(60) Bhosale, S.; Rao, M.; Deshpande, V. *Microbiol. Rev.* **1960**, *60*, 280−300.
(61) Hara, M. *Energy Environ. Sci.* **2010**, *3*, 601−607.
(62) Kuster, B. F. M. *Starch* **1990**, *42*, 314−321.
(63) Binkley, R. W.; Binkley, W. W.; Grey, A. A. *Carbohydr. Res.* **1973**, *28*, 365−370.
(64) Binkley, R. W.; Binkley, W. W.; Wickberg, B. *Carbohydr. Res.* **1974**, *36*, 196−200.
(65) Hamada, K.; Yoshihara, H.; Suzukamo, G.; Hiroaki, O. *Bull. Chem. Soc. Jpn.* **1984**, *57*, 307−308.
(66) Defaye, J.; Gadelle, A.; Pedersen, C. *Carbohydr. Res.* **1985**, *136*, 53−65.
(67) Van-Dam, H. E.; Kieboom, A. P. G.; Van-Bekkum, H. *Starch* **1986**, *38*, 95−101.
(68) Nikolla, E.; Roman-Leshkov, Y.; Moliner, M.; Davis, M. E. *ACS Catal.* **2011**, *1*, 408−410.

DOI: 10.1021/acscatal.5b00559
ACS Catal. 2015, 5, 4761−4771